Sustainable Energy Technologies and Assessments 54 (2022) 102832

Contents lists available at ScienceDirect

Sustainable Energy Technologies and Assessments

journal homepage: www.elsevier.com/locate/seta

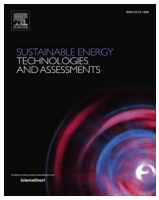

Thermoeconomic assessments and optimization of a vapour compression and an ejector integrated sCO_2 trigeneration systems

Tuğberk Hakan Çetin, Jie Zhu *

Department of Architecture and Built Environment, University of Nottingham, University Park, Nottingham NG7 2RD, UK

ARTICLE INFO

Keywords:
sCO_2 recuperation
Trigeneration
Vapour compression
Ejector cycle
Thermoeconomics

ABSTRACT

Two sCO_2 trigeneration systems are proposed in this study to supply power, heating and cooling simultaneously, one is a vapour compression recuperation system (VCRS), the other is an ejector integrated recuperation system (EIRS). Their performance assessments are conducted from thermoeconomic point of view. In a recuperative base case scenario with cooling capacity of 100 kW, the transcritical VCRS has the ability to provide 46.5 kW power output with the trigeneration utilization efficiency of 160 % and exergy efficiency of 49.92 %, while the transcritical EIRS can deliver 54.43 kW power with the trigeneration utilization efficiency of 158 % and exergy efficiency of 54.41 %. The effects of key operational parameters are evaluated, including the maximum cycle pressure, minimum and maximum power cycle temperatures, evaporation temperature and trade-offs between thermoeconomic points. Multi-objective optimization is carried out based on the identified trade-offs. It is found that the VCRS exergy efficiency increases 4.51 % when the minimum exergy cost rate rises 13 %, the EIRS exergy efficiency improves 4.21 % as the minimum exergy cost rate goes up 14 %.

Introduction

Buildings account for 40 % of the total primary energy consumption and 36 % of greenhouse emission during the pre-pandemic era [1]. As the pandemic changes the daily life routines, electricity demand increases sharply [2] and leads up to 182 % increase in carbon emission [3]. Although the Covid-19 opens up new areas for future energy technology, energy-efficient supply ways would lessen the weight of climate mitigation difficulty. Multiple energy generations by combining cooling, heating and power (CCHP) are widely accepted to reduce this burden [4].

Owing to the sheer CO_2 properties, such as environmental friendliness, wide availability, safety and thermal stability, using CO_2 in the CCHP system has attracted a lot of attention [5,6]. The low critical point of CO_2 (31.0 °C and 7.38 MPa) allows the use of its supercritical capabilities in power generation. Currently most researches on sCO_2 system focus on large scale applications, such as concentrated solar power (CSP) [7], 4th generation nuclear power plant [8], coal fired power plant [9], and bottoming cycle for waste heat recovery with gas turbine [10]. On the other hand, there are extensive researches on the transcritical CO_2 system for the CCHP application. Wang et al. [5] proposed a solar powered Brayton cycle integrated with ejector cooling to provide cooling, heating and electricity, they discovered that the cycle has a trigeneration efficiency of 53 % and a exergy efficiency of 28 % while delivering 7.9 kW cooling and 63.5 kW heating output. Vutukuru et al. [11] presented a tri-generation system by integrating a recuperative Brayton cycle with a transcritical ejector cycle, and investigated the system thermodynamic performance for diary application. They found the system can provide 80.4 kW cooling and 283.49 kW heating while having 7.07 kW net power output.

Energy system designs are normally based on the available energy sources. For the low temperature heat sources below 300 °C, the organic Rankine cycle is favourable, but for the high temperature heat sources above 300 °C, the supercritical CO_2 technology is preferable [12]. Employing CO_2 supercritical properties in the cycle leads to low compression work due to its high density and high thermal efficiency [13]. Currently ongoing researches on power generation with sCO_2 target on medium-large scale systems. Li et al. [14] carried out thermodynamic assessments of six different sCO_2 layouts for waste heat recovery, and found that partial heating cycle is the most promising from thermodynamics second law point of view with exergy efficacy of 55.08 %, but simple recuperative cycle is the most suitable from cycle simplicity aspect. Marchionni et al. [15] investigated eight variants of sCO_2 Joule-Brayton cycle, and discovered that complex variants reach high exergy efficiency up to 45 %, and recompression cycle can achieve

* Corresponding author.
E-mail address: jie.zhu@nottingham.ac.uk (J. Zhu).

https://doi.org/10.1016/j.seta.2022.102832
Received 9 June 2022; Received in revised form 6 October 2022; Accepted 10 October 2022

Nomenclature

$\dot{C}$	exergy cost rate ($/h)
C	specific exergy cost($/GJ)
EIRS	ejector integrated recuperation system
Ejc	ejector
$\dot{E}x$	exergy (kW)
Ex	specific exergy (kJ/kg)
H	specific enthalpy(kJ/kg)
$\dot{m}$	mass flow rate (kg/s)
P	Pressure (MPa)
PR	Pressure Ratio
$\dot{Q}$	heat transfer rate (kW)
S	entropy (kW/K)
S	specific entropy(kJ/kg.K)
T	temperature (°C or K)
V	velocity(m/s)
Vcc	vapour compression cycle
VCRS	vapour compression recuperation system
$\dot{W}$	power (kW)
Z	cost of component ($)
$\dot{Z}$	Levelized cost rate of component ($/h)

Greek Letters

Δ	difference
E	exergy efficiency
H	energy efficiency
M	entrainment ratio

Subscripts and indices

1,2,3	states
Ac	air cooler
D	destruction
D	diffuser
Evap	evaporator
F	fuel
Gh	gas heater
M	mixing
N	nozzle
P	products
S	isentropic
Spc	space heating

the specific cost of 1775 $/kW$_e$.

Integration of sCO_2 power cycle with cooling technology is getting more popular recently. Zhang et al. [16] proposed different power and cooling configurations by changing integration of a transcritical ejector and compression cooling cycle with single and dual stage compression Brayton cycles for refrigerated truck application. Their results show that, the ejector cooling cycle with single stage compression increases power output by 4.9 % and exergy efficiency by 22.8 % under refrigeration mode, while the system with dual compression cycle increases power output by 18 % and efficiency by 14.7 %. Yuan et al. [17] developed an ejector integrated recompression cycle powered by nuclear energy for combined cooling and power (CCP) application, and found that the cycle can supply 43.10 MW power and 10.92 MW cooling with exergy efficiency of 61.07 %. In the another study of Yuan et al. [18], they proposed four different configurations for ejector and vapour compression integrated sCO_2 systems that can operate under three operation modes: power only, power and cooling simultaneously, and cooling only modes. They presented the maximum ratio of cooling capacity over heat input is 1.714. Wang et al. [19] investigated the ejector and vapour compression integrated recuperative transcritical systems driven by low grade thermal source, and claimed that for the turbine inlet temperature of 220 °C, the vapour compression integrated system can produce net power output of 7537.5 kW with exergy efficiency of 26.9 % while the ejector integrated system can provide net power output of 7910.3 kW with exergy efficiency of 27.7 %.

Currently, most researches on the sCO_2 cycle are based on vapour compression and ejector refrigeration integrated CCP and CCHP systems to investigate system performance from energy and exergy aspects, and economic point of view, there is the lack of study considering thermoeconomics of such systems. This study aims to fill this research gap by conducting comprehensive thermoeconomic analyses of the transcritical vapour compression and ejector integrated recuperative sCO_2 systems. For this purpose, thermoeconomic relations for the two systems are formulated. In the base case scenario, the systems' performance under the same cooling load are explored. Comprehensive parametric studies are also carried out to investigate the system operational parameter effects on thermoeconomic performance. Lastly, multi-objective optimization is performed to maximize exergy efficiency and minimize exergy cost rate of products.

System description

The proposed vapour compression sCO_2 recuperation system (VCRS) is given in Fig. 1a). The system is formed by combing a compression cooling cycle and a sCO_2 power cycle, the main components include a gas heater, a micro turbine, a recuperator, a main compressor, a space/hot water heat exchanger, an air cooler, an electric compressor, an evaporator and a expansion valve. In the VCRS, high temperature sCO_2 stream leaving the gas heater at state 1 expands in the turbine, then heats the upcoming high pressure sCO_2 from the main compressor (stream 8–9) in the recuperator. The stream leaving the recuperator hot side (state 3) mixes with the one from the electric compressor. The mixed stream supplies heating to users and is cooled down in the air cooler further. Afterwards the stream is split into two parts, one part of the stream is diverted into the power cycle while the other stream is diverted into the vapour compression cycle. The stream diverted into the power cycle flows into the main compressor to increase its pressure, then the high pressure stream is heated in the recuperator and gas heater to reach high temperature, the high pressure and temperature stream (state 1) goes into the turbine for power generation, The stream diverted into the vapour compression cycle expands through the expansion valve (state 11) and absorbs heat to produce cooling effect, then is compressed by the electric compressor (state 13) to reach the same pressure as that of the stream leaving the recuperator (state 3), and merges with the stream in the power cycle.

The proposed ejector integrated sCO_2 recuperation system (EIRS) is presented in Fig. 1b). Two more components are added in the EIRS compared with the VCRS, they are an ejector and a separator. The working principle of the EIRS is similar to that of the VCRS except on the cooling aspect. One split stream (state 10) from the air cooler is used as the primary flow in the ejector to entrain the secondary flow from the evaporator. Intermediate pressure stream leaving the ejector (state 16) enters the separator where the liquid phase stream (state 18) is diverted into the expansion valve to expand and then absorbs heat to produce cooling while the vapour phase stream (state 17) is diverted to the electric compressor to be compressed and mixed with the stream leaving the recuperator.

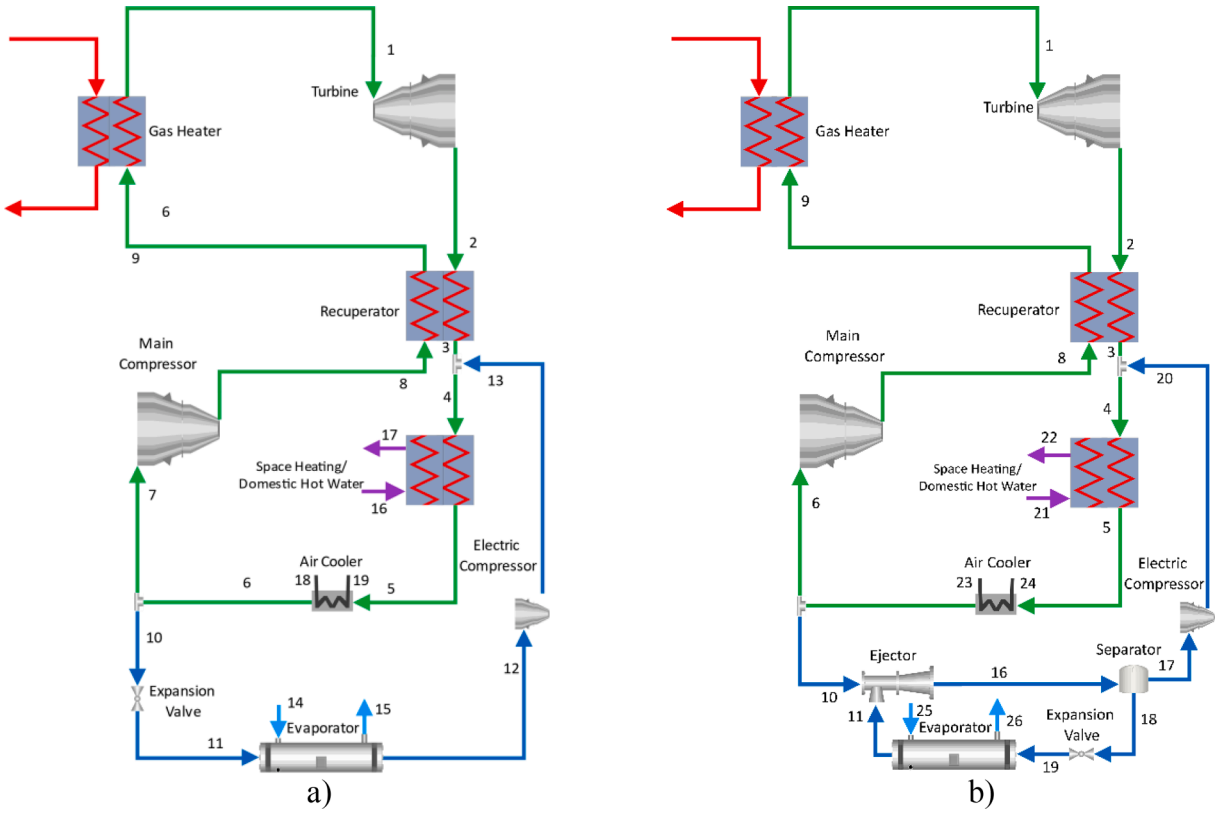

Fig. 1. Schematic diagrams of a) Vapour compression sCO_2 recompression system (VCRS) b) Ejector integrated sCO_2 recompression system (EIRS).

System modelling

Thermodynamic models

The system performance is investigated according to thermodynamics first and second laws, which gives us both qualitative and quantitative information about system operating characters [20]. Fundamental governing equations used in this study are stated as follows

$$\sum \dot{m}_i = \sum \dot{m}_e \tag{1}$$

$$\sum \dot{Q} - \sum \dot{W} = \sum \dot{m}_e h_e - \sum \dot{m}_i h_i \tag{2}$$

$$\sum S_i - \sum S_e + S_{gen} = 0 \tag{3}$$

where $\dot{m}$ denotes the mass flow rate of the fluid, $\dot{Q}$ and $\dot{W}$ are the rates of heat input and power output respectively, h is the specific enthalpy and S is the entropy.

In the exergy analysis, physical exergies of all streams are taken into account and "exergy fuel/exergy products" concept is applied [21]. Exergy balances for each component and overall system are written as follows.

$$\dot{E}x_F = \dot{E}x_P + \dot{E}x_D \tag{4}$$

where subscripts F, P and D indicate the fuel, products and destruction respectively.

The exergy of heat transfer at temperature T is expressed as [22]:

$$\dot{E}x_q = \sum (1 - \frac{T_0}{T})\dot{Q} \tag{5}$$

Physical exergy of each stream is expressed as:

$$ex = (h - h_0) - T_0(s - s_0) \tag{6}$$

where 0 subscript stands for the dead state.

The system models are complex owing to many components, and variable thermal and physical properties, in order to simplify the system mathematical models, the following assumptions are adopted [18,19]:

- The system operates at the steady state.
- Chemical, kinetic and potential energy changes are neglected.
- Pressure drop in pipe and heat loss to the environment are not considered.
- The flow across the throttle valve is isenthalpic.
- The outlet working fluid of the evaporator is the saturated vapour.
- The flow inside the ejector is one-dimension.
- The ejector inlet velocities of the primary and secondary fluids are negligible.
- The efficiencies of the turbine and compressors for power cycle are fixed.

VCRS thermodynamic model

The isentropic efficiencies of the turbine and main compressor are taken as 0.8 and 0.7 respectively, while the isentropic efficiency of the electric compressor $\eta_{elec,comp}$ is calculated from the following equation [23].

$$\eta_{elec,comp} = \frac{h_{o,s} - h_i}{h_o - h_i} = 0.004762PR^2 - 0.09238PR + 0.8910 \tag{7}$$

where subscripts i and o indicate the compressor inlet and outlet, s represents the ideal isentropic state, and PR is the pressure ratio of compressor.

Equations (1), (2) and (3) are applied to both the system and each component. For exergy analysis, fuel and products approaches are adopted. Fuel and products exergies for each component in the VCRS are given in the appendix Table A1.

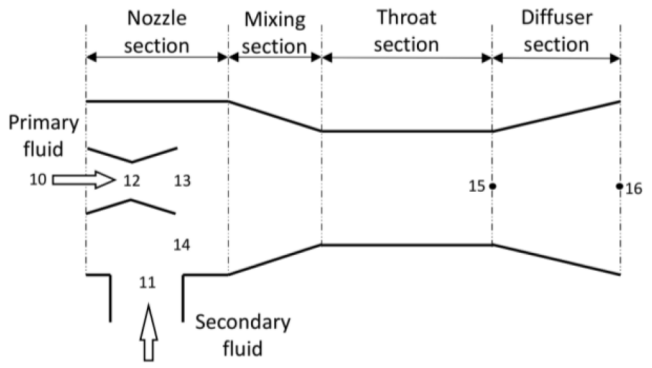

Fig. 2. Schematic diagram of the ejector.

EIRS thermodynamic model

For modelling a transcritical ejector, the comprehensive model based on mass, momentum and energy conservation equations and flow properties is adopted [24], the ejector schematic diagram with corresponding states is given in Fig. 2. Some approximations are made so as to employ the ejector model, the main assumptions are in below.

- Isentropic efficiencies are adopted for the nozzle and diffuser.
- Choked condition is taken into account for the primary nozzle.
- Constant pressure mixing model is used in the ejector.
- Loss in the mixing chamber is considered with a mixing efficiency.

The outlet velocity of the primary fluid from the nozzle is formulated as:

$$V_{13} = \sqrt{2(h_{10} - h_{13})} \tag{8}$$

where h_{13} is the outlet enthalpy at the throat and calculated as:

$$h_{13} = h_{10} - \eta_{prim}(h_1 - h_{13,s}) \tag{9}$$

where $h_{13,s}$ is the outlet enthalpy for the isentropic flow, η_{prim} is the isentropic efficiency of the primary nozzle convergent section.

Based on momentum conservation principle, the mixing velocity is expressed as follows:

$$V_{15} = \varphi_{mix}\frac{V_{13} + \mu V_{14}}{1+\mu} \tag{10}$$

where φ_{mix} is the mixing coefficient. The outlet enthalpy of the mixing chamber is calculated as:

$$h_{15} = \frac{1}{1+\mu}\left(h_{13} + \frac{{V_{13}}^2}{2}\right) + \frac{\mu}{1+\mu}\left(h_{14} + \frac{{V_{14}}^2}{2}\right) - \frac{{V_{15}}^2}{2} \tag{11}$$

where μ is the ejector entrainment ratio and defined as the ratio of the secondary fluid mass flow rate over the primary fluid mass flow rate.

For the diffuser section, the enthalpy of the diffuser outlet is expressed as:

$$h_{16} = h_{15} - \frac{h_{16,s} - h_{15}}{\eta_{diff}} \tag{12}$$

And the outlet velocity of the diffuser is calculated from:

$$V_{16} = \sqrt{2(h_{15} - h_{16}) + {V_{16}}^2} \tag{13}$$

Fuel and products exergies for each component in the EIRS are given in the appendix Table A2.

Thermoeconomic models

In order to assess the system performance from financial aspect, the system economic and thermoeconomic studies are conducted. The main goal of the economic analysis is to provide the product cost, while thermoeconomic analysis presents inefficiencies of the system and costs of these inefficiencies [25].

For economic analysis, the total cost rate of each component is the sum of capital investment, and operation and maintenance cost rates, it is expressed as follows:

$$\dot{Z}_k = \dot{Z}_k^{CI} + \dot{Z}_k^{O\&M} \tag{14}$$

where $\dot{Z}_k^{CI}$ is the annual levelized capital investment rate and $\dot{Z}_k^{O\&M}$ is the operation and maintenance cost rate.

The annual levelized capital cost rate is expressed as follows:

$$\dot{Z}_k^{CI} = \frac{CRF}{\tau} Z_k \tag{15}$$

where Z_k is the capital cost of the kth component, τ is the annual plant operation hours. The CRF is the capital recovery factor and written as:

$$CRF = \frac{i(1+i)^n}{(1+i)^n - 1} \tag{16}$$

where i is the interest rate and n is the plant life time in years.

Annual levelized operation and maintenance cost rate is calculated from:

$$\dot{Z}_k^{O\&M} = \frac{\gamma_k Z_k}{\tau} \tag{17}$$

where γ_k is the maintenance factor.

The cost functions for key components are given in the appendix Table A3.

Thermoeconomic analysis is carried out based on the specific exergy costing (SPECO) method [26]. The SPECO method is applied in three steps: (1) identification of exergy streams, (2) definitions of fuel and

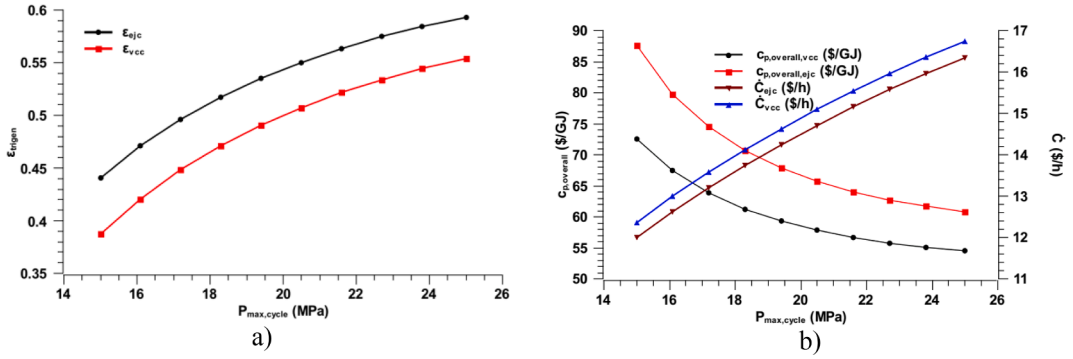

Fig. 3. Effects of the maximum pressure on a) exergy efficiency b) exergy cost rate and specific exergy cost of products.

products of each component, and (3) applying cost-balance equation for each component.

For the component receiving heat and generating power, its cost balance is written as:

$$\dot{C}_w + \sum \dot{C}_e = \dot{C}_q + \sum \dot{C}_i + \dot{Z}_k \tag{18}$$

where $\dot{C}_w$, $\dot{C}_e$, $\dot{C}_q$, and $\dot{C}_i$ are the exergetic cost rates associated with work, exiting streams, heat transfer and entering streams, and expressed as following:

$$\dot{C}_w = c_w \dot{W} \tag{19}$$

$$\dot{C}_q = c_q \dot{E}x_q \tag{20}$$

$$\dot{C}_i = c_i \dot{E}x_i \tag{21}$$

$$\dot{C}_e = c_e \dot{E}x_e \tag{22}$$

where "c" is the cost per exergy in $/GJ.

Except unit exergetic cost of the products, thermoeconomic analysis yields three important variables which help to identify inefficiencies and improve overall system performance. They are the cost of exergy destruction $\dot{C}_D$, relative cost difference r_k, and thermoeconomic factor f_k.

The cost of exergy destruction of the kth component is expressed as:

$$\dot{C}_{D,k} = c_{f,k} \dot{E}_{D,k} \tag{23}$$

where $c_{f,k}$ is the fuel unit cost of the kth component.

The relative cost difference identifies the increase in the average cost per exergy unit between fuel and products of component, and is written as follows:

$$r_k = \frac{c_{p,k} - c_{f,k}}{c_{f,k}} \tag{24}$$

where $c_{p,k}$ is the products unit cost of the kth component.

The cost sources for each component can be divided in two categories, one is the cost related to the initial investment, operation and maintenance costs, and the other is the cost related to the exergy destruction. Thermoeconomic factor f_k is defined to identify the ratio of these two costs and can be written as:

$$f_k = \frac{\dot{Z}_k}{\dot{Z}_k + \dot{C}_{D,k}} \tag{25}$$

Performance indicators and Multi-Objective optimization

The system trigeneration efficiency is expressed as:

$$\eta_{trigen} = \frac{(\dot{W}_{net} + \dot{Q}_{spc} + \dot{Q}_{evap})}{\dot{Q}_{gh}} \tag{26}$$

where $\dot{Q}_{gh}$ is the heat input from the gas heater, $\dot{Q}_{spc}$ is the heat released for space heating, and $\dot{Q}_{eva}$ is the heat absorbed for producing cold. $\dot{W}_{net}$ is the net power output and can be expressed in terms of power produced by the turbine and power consumed by main and electric compressors.

$$\dot{W}_{net} = \dot{W}_{turb} - \dot{W}_{comp} - \dot{W}_{comp,el} \tag{27}$$

Exergetic efficiency is expressed as the ratio of the sum of net power output and exergy output from the space heater and evaporator over the exergy input in the gas heater:

$$\varepsilon_{trigen} = \frac{\dot{W}_{net} + \dot{E}x_{spc} + \dot{E}x_{evap}}{\dot{E}x_{in}} \tag{28}$$

The levelized cost of energy (LCOE) is expressed as:

$$\text{LCOE} = \frac{\dot{Z}_{total} + \dot{C}_q}{\dot{W}_{net} + \dot{Q}_{spc} + \dot{Q}_{eva}} \tag{29}$$

where $\dot{Z}_{total}$ is the sum of component cost rates.

Equation (18) can be rewritten for the overall system:

$$\dot{C}_{p,overall} = \dot{C}_{f,overall} + \dot{Z}_{total} \tag{30}$$

Where $\dot{C}_{p,overall}$ is the overall cost rate of products in the system and $\dot{C}_{f,overall}$ is the overall cost rate of fuel of the system.

Unit cost of products exergy is expressed as following:

$$c_{p,overall} = \frac{\dot{C}_q + \dot{Z}_{total}}{\dot{W}_{net} + \dot{E}x_{spc} + \dot{E}x_{evap}} \tag{31}$$

For multi-objective optimization, the exergy efficiency ε_{trigen} will be maximized and cost rate of exergy products $c_{p,over}$ will be minimized. Normally the optimization problem can be expressed as follows:

$$Min_x\{-\varepsilon_{trigen}, \dot{C}_{p,overall}\} \tag{32}$$

Where x is the vector of

$$x = \{P_{min}, P_{max}, \Delta T_{min}, T_{evap}, T_{max}, T_{min}\} \tag{33}$$

Subject to

$$7.6MPa < P_{min} < 10MPa \tag{34}$$

$$15\,MPa < P_{max} < 25\,MPa \tag{35}$$

$$3^{\circ}\text{C} < \Delta T_{min} < 15^{\circ}\text{C} \tag{36}$$

$$-15^{\circ}\text{C} < T_{evap} < 5^{\circ}\text{C} \tag{37}$$

$$400^{\circ}\text{C} < T_{max} < 800^{\circ}\text{C} \tag{38}$$

$$32.3^{\circ}\text{C} < T_{min} < 35^{\circ}\text{C} \tag{39}$$

Non-dominated sorting genetic algorithm II (NSGA-II) method is used to solve the multi-objective optimization problem [27,28]. The control parameters for algorithm are specified with population size of 50, number of generations of 300 and crossover fraction of 0.8 [29].

Results and discussion

The performance of the VCRS and EIRS are evaluated from energy, economics and thermoeconomic points of view. Parametric analyses are carried out to explore the effects of key operating parameters including the minimum cycle temperature and pressure, maximum cycle temperature and pressure, and evaporation temperature, on the system thermoeconomic performance. Result of the base case scenario is given in the Appendix A-3.

Effects of the maximum cycle pressure

Variations of the system exergy efficiency, exergy cost rate and specific exergy cost of products with the maximum cycle pressure are given in Fig. 3a) and b) respectively. When the pressure changes from 15 MPa to 25 MPa, the specific costs of exergy of products increase from 87.57$/GJ and 72.75$/GJ to 60.86$/GJ and 54.53$/GJ for the VCRS and EIRS respectively. This is because the turbine expansion ratio, cycles' net power output and exergy efficiency increase with the maximum pressure, these lead to the decrease in specific cost of exergy of products. As the specific exergy cost of products decreases, the exergy cost rates of products reach up to 16.73$/h and 16.34$/h for the VCRS and EIRS respectively, due to the size increases of the turbine, recuperator and main compressor.

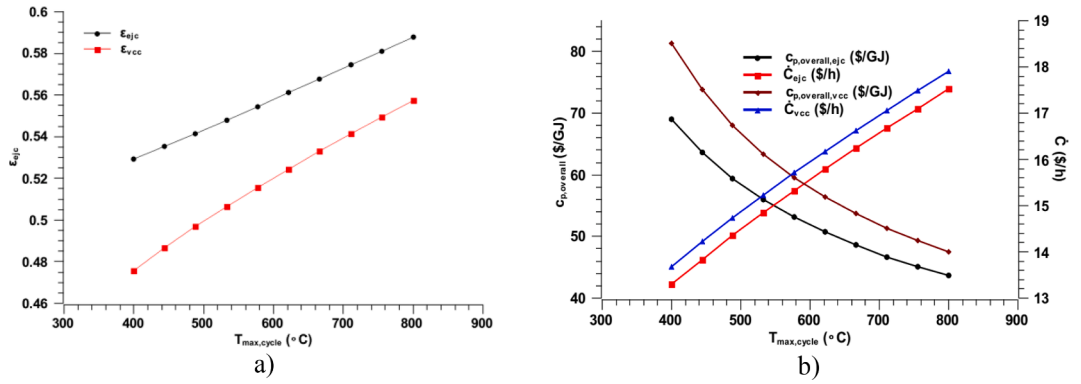

Fig. 4. Effects of the maximum cycle pressure on a) exergy efficiency b) exergy cost rate and specific exergy cost of products.

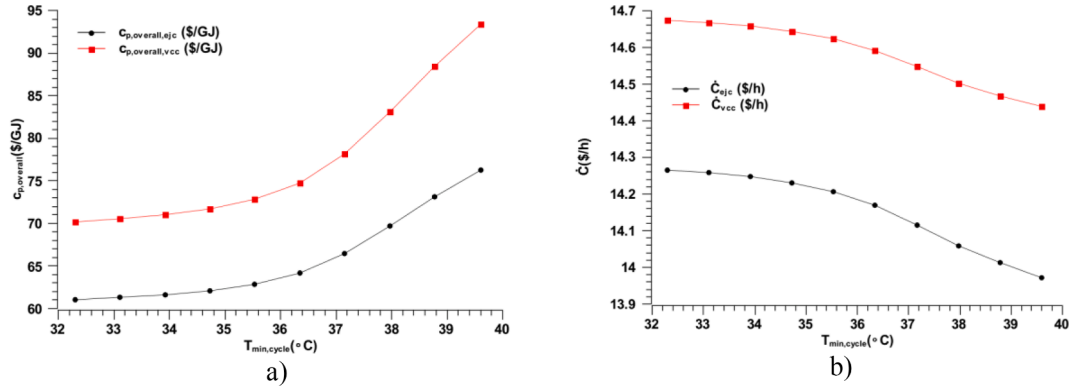

Fig. 5. Effects of the minimum cycle temperature on a) specific exergy cost of products and b) exergy cost rate.

Effects of the maximum cycle temperature

Variations of exergy efficiency, exergy cost rate and specific exergy cost of products with the maximum cycle temperature are shown in Fig. 4 a) and b), respectively. As the maximum cycle temperature changes from 400 °C to 800 °C, the exergy efficiencies increase from 47.55 % to 55.74 % for the VCRS and from 52.91 % to 58.76 % for the EIRS, these improvements are caused by the turbine high inlet temperature. The exergy cost rates increase from 13.68$/h to 17.90$/h for the VCRS and from 13.29$/h to 17.52$/h for the EIRS. The maximum cycle temperature influences the thermoeconomic performance in two respects: the sizes of heat transfer equipment and the turbine, and fuel cost. Due to the increases in heat transfer rate and turbine work, equipment sizes are getting bigger, which increase the cost rates of components $\dot{Z}$ and fuel cost of overall cycle $\dot{C}_f$.

Effects of the minimum power cycle temperature

The variations of specific exergy cost of products and exergy cost rate with the minimum power cycle temperature are shown in Fig. 5a) and b), respectively. In general, low compression inlet temperature is favourable to reduce the compressor power consumption. For the case of compression near the CO_2 critical region, it is more obvious since high density of the supercritical fluid leads to compact size and low power consumption [30]. Similarly, the ejector performs better near the critical region with high cooling output. When the air cooler outlet temperature decreases from 40 °C to 32.3 °C, the ejector entrainment ratio increases from 0.5735 to 0.6531 and the system cooling output rises from 43.40 kW to 101.43 kW. The specific exergy costs of products increase from 70.17$/GJ to 93.40$/GJ for the VCRS and from 61.06$/GJ to 76.30 $/GJ for the EIRS. As the compression is away from the supercritical

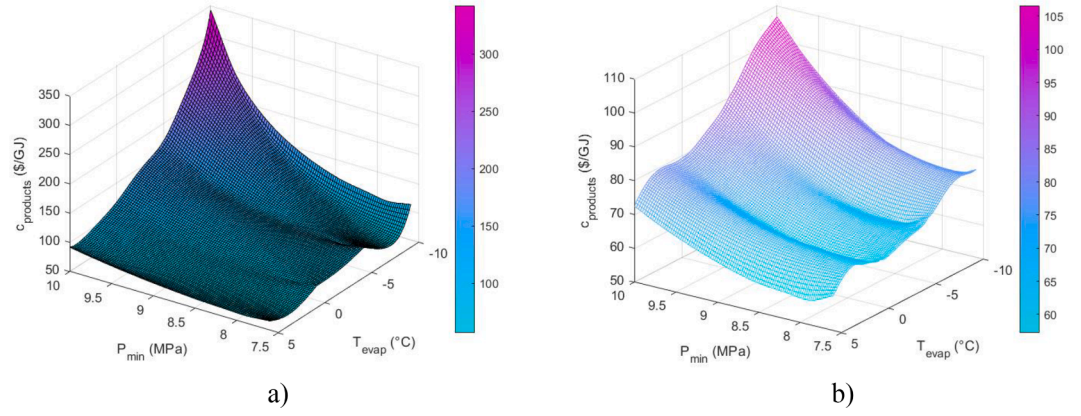

Fig. 6. Variations of the specific exergy cost with the minimum power cycle pressure and evaporation temperature for a) VCRS and b) EIRS.

region, the specific exergy costs of products increase rapidly. The supercritical properties of the working fluid also has a considerable effect on the heat exchanger size. When the temperature decreases from 40 °C to 32.3 °C, the air cooler heat transfer area increases from 1.3m^2 to 10 m^2. When the minimum temperature is 32.3 °C, the exergy cost rates of products reach up to 14.67$/h and 14.26$/h for the VCRS and EIRS respectively.

Combined effects of the minimum power cycle pressure and evaporation temperature

Variations of exergy cost rate with the minimum power cycle pressure and evaporation temperature for the VCRS and EIRS are given in Fig. 6a) and b), respectively. As the minimum cycle pressure increases to 10 MPa and evaporation temperature decreasse to −10 °C, the VCRS specific exergy cost of the products increases up to 342.3$/GJ due to the increase in pressure ratio for the electric compressor, the EIRS specific exergy cost increases up to 106.6$/GJ due to the lower pressure ratio in the electrical compressor as well. As the minimum pressure reduces to 7.6 MPa and evaporation temperature increases up to 5 °C, the lowest values of specific exergy cost of products are achieved with 63.05$/GJ for the VCRS and 57.35$/GJ for the EIRS.

Optimization

In the parametric analyses, trade-offs between the exergy cost rate of products and exergy efficiency are identified. To handle these trade-offs for the best results, multi-objective optimization is conducted. Pareto frontier concept is a very useful tool to identify the best solution for conflicting objective functions, the Pareto efficient solutions are represented in criterion space which allows designer to set the Pareto efficient solutions and focus on trade-offs within the set [31]. In this study, they are exergy efficiency and exergy cost rate of products. For selection of the final optimum solution in the Pareto optimal set, the concept of utopia point is implemented. In this section, the optimization results for both systems are presented.

VCRS optimization

Pareto plot for the VCRS is given in Fig. 7a). As illustrated in Fig. 7, the minimum exergy cost rate of products is 10.72$/h which corresponds to the lowest exergy efficiency value of 30.84 %. The maximum exergy efficiency for this Pareto optimum set is 58.11 % which corresponds to the cost rate of 18.30$/h. As the capital investment rises by 23 %, the exergy efficiency can increase up to 58 %.

Utopia point is identified as where both the exergy efficiency and exergy cost rate reach the optimum values and depicted in Fig. 7. A compromise solution point where is the minimum Euclidean distance between the utopia point and Pareto optimal set, is selected as the final optimum solution [32].

Decision variables and performance parameters corresponding to this point are given in Table 1. In the selected optimum case, the system net power output increases from 46.5 kW to 70.41 kW as the system operates with the maximum cycle temperature of 686 °C and minimum power cycle temperature of 34.83 °C. The energy and exergy efficiencies are 162 % and 54.44 % respectively for the optimum case. While the exergy cost rate increases from 14.87 $/h to 16.80 $/h, the specific exergy cost of products decreases from 66.78$/GJ to 54.29$/GJ. The increases in the fuel cost and component's capital investment cost are compensated by the exergy products.

EIRS optimization

Pareto plot for the EIRS configuration is given in Fig. 7b). As illustrated in Fig. 7b), the minimum cost rate is 10.85$/h with an exergy efficiency of 41.11 %, and the maximum exergy efficiency is 61.94 % which corresponds to the cost rate value of 19.34$/h. As indicated in Fig. 7b), 13 % increase in exergy efficiency can be achieved as the capital investment is enhanced by 21 %. Similarly, the utopia point is identified and depicted in Fig. 8. The compromise solution is selected, and its performance data are presented in Table 1. Compared with the base case scenario in selected optimum operation, the EIRS net work output increases from 54.43 kW to 71.83 kW and space heating output increases from 241 kW to 281.94 kW while the system operates under the maximum pressure of 23.72 MPa and evaporation temperature of 2.72 °C. Under this operating condition, the energy and exergy efficiencies are 158 % and 58.62 % respectively. When the cost rate rises from 14.52$/h to16.62$/h, the specific exergy cost of products decreases from 58.14$/GJ to 52.46$/GJ and the exergy efficiency increases from 54.41 % to 58.62 %.

Performance comparison

To conduct comprehensive thermoeconomic comparison with similar systems, the results of this study are compared with those of an ejector boosted sCO_2 trigeneration system [33], an Organic Rankine Cycle (ORC) based absorption trigeneration system [34], and a vapour compression integrated ORC trigeneration system [35]. The energy efficiency of the ejector boosted sCO_2 trigeneration system with 100 kW cooling output is 163 %, while the EIRS can achieve energy efficiency of 168 % under the same cooling output. The ORC based absorption trigeneration system has a net work output of 50 kW with exergy efficiency of 44.19 % and exergy cost rate of 12.72$/h, under the same size and optimum operating conditions, the VCRS reaches exergy efficiency of 51.93 % and exergy cost rate of 12.76$/h, and the EIRS achieves exergy efficiency of 56.43 % and exergy cost rate of 11.97$/h, so the exergy efficiencies of the VCRS and EIRS are increased 7.74 % and 12.24 % respectively, compared with that of the ORC based absorption

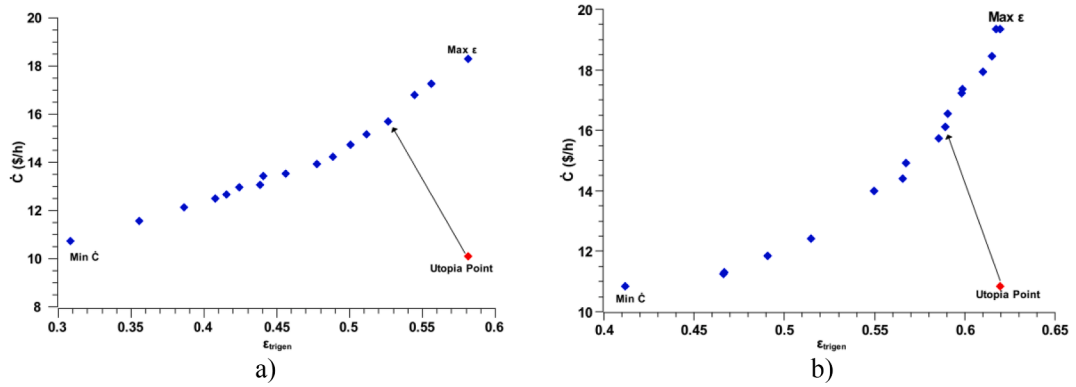

Fig. 7. Pareto plots for the a) VCRS b) EIRS.

trigeneration system. Under the same cooling output of 303 kW, the vapour compression integrated ORC trigeneration system operates with exergy efficiency of 40.57 % and specific cost of products of 49.84$/GJ, the VCRS runs with exergy efficiency of 52.03 % and specific cost of products of 54.12$/GJ, the EIRS works with exergy efficiency of 56 % and specific cost of products of 51.12$/GJ, therefore the exergy efficiencies of the VCRS and EIRS are improved 11.46 % and15.43 % compared with that of the vapour compression integrated ORC trigeneration system. These comparisons demonstrate that both the VCRS and EIRS have high energy and exergy efficiencies, and competitive exergy cost rate and specific cost of products.

Conclusions

Thermoeconomic assessments and optimization of two trigeneration systems are carried out in this study. The influences of key operational parameters on the overall thermoeconomic performance are clarified. The following conclusions can be drawn from the results of this study:

- Recuperator is the highest contributor of the cost of exergy destruction rate for both systems, due to the high irreversibility rate in the heat transfer process.
- Overall cost of exergy destruction rate for the EIRS is 2838.14$/h, which is lower than the VCRS 3595.28$/h. This is because using an ejector as the main expansion device reduces irreversibility in the expansion process.
- In the EIRS, the ejector entrainment ratio, cooling output and products specific exergy cost increase as the air cooler temperature decreases. When the air cooler outlet temperature drops from 40 °C to 32.3 °C, the ejector entrainment ratio grows from 0.5735 to 0.6531, the cooling output increases from 43.40 kW to 101.43 kW, and the products specific exergy cost rises from 61.06$/GJ to 76.30 $/GJ.
- The exergy efficiencies of both systems improve with the exergy cost rate, but their specific exergy costs of products reduce with it. In the selected optimum solutions, the VCRS exergy efficiency increases from 49.92 % to 54.43 % and specific exergy cost of products decreases from 66.71$/GJ to 55.76$/GJ as the exergy cost rate changes from 14.87$/h to 16.80$/h, while the EIRS exergy efficiency increases from 54.41 % to 58.62 % and specific exergy cost of products decreases from 58.14$/GJ to 52.46$/GJ when the exergy cost rate rises from 14.52$/h to 16.62$/h.
- The maximum exergy efficiency varies with the exergy cost rate. The VCRS maximum exergy efficiency of 54.43 % is achieved when the exergy cost rate is 16.80 $/h, the EIRS maximum exergy efficiency of 61.94 % is reached as the exergy cost rate is 19.34$/h.

The minimum exergy cost rate and lowest exergy efficiency can be attained simultaneously. The VCRS minimum exergy cost rate is 10.72 $/h which corresponds to the lowest exergy efficiency value of 30.84 %, and the EIRS minimum exergy cost rate is 10.85$/h which corresponds to the lowest exergy efficiency value of 41.19 %.The proposed thermoeconomic model is designed for general case so it can be applied to any heat source to power the system. The thermoeconomic study shows that, due to the high irreversibility in the VCRS, the EIRS has better thermoeconomic performance. Also, the EIRS performs better under low evaporation temperature which makes it more suitable for cold climate application. In the future, district level application of these systems under realistic electrical and thermal loads will be investigated.

CRediT authorship contribution statement

Tuğberk Hakan Çetin: Conceptualization, Methodology, Software, Visualization. **Jie Zhu:** Conceptualization, Methodology, Supervision.

Declaration of Competing Interest

The authors declare that they have no known competing financial interests or personal relationships that could have appeared to influence the work reported in this paper.

Data availability

Data will be made available on request.

Acknowledgment

The financial supports from TUBITAK under 2213/A-Overseas Graduate Scholarship Program is gratefully acknowledged by Authors

Appendix A:. Supplementary tables and figures

A-1 Exergy analysis

In this study, fuel and product concept for exergy analysis are adopted in order to facilitate thermoeconomic analysis. Fuel and product expressions for the VCRS and EIRS are given in Table A1 and Table A2, respectively.

Table 1
The optimum solutions for the VCRS and EIRS.

Decision variable	VCRS	EIRS	Performance parameter	VCRS	EIRS
Minimum cycle pressure P_{min} (MPa)	8.565	8.64	W_{net} (kW)	70.41	71.83
Maximum cycle pressure P_{max} (Mpa)	20.734	23.72	$\dot{Q}_{gh}$ (kW)	266.58	281.94
Maximum cycle temperature T_{max} (°C)	686	568.63	$\dot{Q}_{spc}$ (kW)	269.16	276.68
Minimum power cycle temperature T_{min} (°C)	34.83	33.9	$\dot{Q}_{evap}$ (kW)	92.46	97.46
Minimum temperature difference recuperator ΔT_{min} (°C)	3.87	6.82	η_{trigen} (%)	162	158
Evaporation temperature T_{evap} (°C)	4.71	2.72	ε_{trigen} (%)	54.44	58.62
			c_p ($/GJ)	54.29	52.46
			$\dot{C}_p$ *($/h)*	16.8	16.62
			LCOE ($/kWh)	0.0389	0.0373

Table A1
Fuel and product exergy expressions for the VCRS.

Component	Fuel exergy	Products exergy
Turbine	$\dot{E}x_1 - \dot{E}x_2$	$\dot{W}_{turb}$
Recuperator	$\dot{E}x_2 - \dot{E}x_3$	$\dot{E}x_9 - \dot{E}x_8$
Mixer	$\dot{E}x_3 + \dot{E}x_{13}$	$\dot{E}x_4$
Space Heater	$\dot{E}x_4 - \dot{E}x_5$	$\dot{E}x_{17} - \dot{E}x_{16}$
Air Cooler	$\dot{E}x_5 - \dot{E}x_6$	$\dot{E}x_{19} - \dot{E}x_{18}$
Main Compressor	$\dot{W}_{comp}$	$\dot{E}x_8 - \dot{E}x_7$
Valve	$\dot{E}x_{10}$	$\dot{E}x_{11}$
Evaporator	$\dot{E}x_{11} - \dot{E}x_{12}$	$\dot{E}x_{15} - \dot{E}x_{14}$
Electric Compressor	$\dot{W}_{comp,el}$	$\dot{E}x_{13} - \dot{E}x_{12}$
Gas Heater	$\dot{E}x_q$	$\dot{E}x_1 - \dot{E}x_9$

Table A2
Fuel and products exergy expressions for the EIRS.

Component	Fuel exergy	Products exergy
Turbine	$\dot{E}x_1 - \dot{E}x_2$	$\dot{W}_{turb}$
Recuperator	$\dot{E}x_2 - \dot{E}x_3$	$\dot{E}x_9 - \dot{E}x_8$
Mixer	$\dot{E}x_3 + \dot{E}x_{20}$	$\dot{E}x_4$
Space Heater	$\dot{E}x_4 - \dot{E}x_5$	$\dot{E}x_{22} - \dot{E}x_{21}$
Air Cooler	$\dot{E}x_5 - \dot{E}x_6$	$\dot{E}x_{24} - \dot{E}x_{23}$
Main Compressor	$\dot{W}_{comp}$	$\dot{E}x_8 - \dot{E}x_7$
Ejector	$\dot{E}x_{10} + \dot{E}x_{11}$	$\dot{E}x_{16}$
Valve	$\dot{E}x_{18}$	$\dot{E}x_{19}$
Evaporator	$\dot{E}x_{19} - \dot{E}x_{11}$	$\dot{E}x_{26} - \dot{E}x_{25}$
Separator	$\dot{E}x_{16}$	$\dot{E}x_{18} + \dot{E}x_{17}$
Electric Compressor	$\dot{W}_{comp,el}$	$\dot{E}x_{20} - \dot{E}x_{17}$
Gas Heater	$\dot{E}x_q$	$\dot{E}x_1 - \dot{E}x_9$

A-2 Economic analysis

For the economic analysis, purchased costs of components are calculated from cost functions given in Table A3.

Table A3
Cost function of component [36–38].

Component	Cost function
Cost of Turbine $Z_{turbine}$ ($)	$7790\ \dot{W}_{turb}^{0.6842}$
Cost of Compressors $Z_{compressor}$ ($)	$6698\ \dot{W}_{comp}^{0.7865}$
Cost of Recuperator $Z_{recuperator}$ ($)	$2681\ A_{rec}^{0.59}$
Cost of Evaporator Z_{evap} ($)	$1397\ A_{evap}^{0.89}$
Cost of Space Heater Z_{spc} ($)	$1930\ A_{spc}^{0.68}$
Cost of Valve Z_{valve} ($)	$114.5\dot{m}_{valve}$
Cost of Ejector $Z_{ejector}$ ($)	$13.5\dot{m}_{primary}\left(\frac{T_{primary}}{P_{primary}}\right)^{0.05}\left(P_{ejc.out}\right)^{-0.75}$
Cost of Gas Heater Z_{gh} ($)	$2681\ A_{gh}^{0.68}$

A-3 Thermoeconomic analysis

A-3.1 VCRS thermoeconomic model

11 equations with 23 unknowns are generated by applying cost balance to each component in the VCRS. To solve these equations by the SPECO method, the auxiliary equations are needed. The cost balance and auxiliary equations of the VCRS are given in Table A4.

Table A4
Cost balance and auxiliary equations for the VCRS.

Component	Cost balance	Auxiliary equations
Turbine	$\dot{C}_2 + \dot{C}_{w,turb} = \dot{C}_1 + \dot{Z}_{turb}$	$\frac{\dot{C}_2}{\dot{E}x_2} = \frac{\dot{C}_1}{\dot{E}x_1}$
Recuperator	$\dot{C}_3 + \dot{C}_9 = \dot{C}_2 + \dot{C}_8 + \dot{Z}_{rec}$	$\frac{\dot{C}_3}{\dot{E}x_3} = \frac{\dot{C}_2}{\dot{E}x_2}$
Mixer	$\dot{C}_4 = \dot{C}_{13} + \dot{C}_3$	–
Space Heater	$\dot{C}_5 + \dot{C}_{17} = \dot{C}_4 + \dot{C}_{16} + \dot{Z}_{spc}$	$\frac{\dot{C}_{17}}{\dot{E}x_{17}} = \frac{\dot{C}_{16}}{\dot{E}x_{16}}, \frac{\dot{C}_4}{\dot{E}x_4} = \frac{\dot{C}_5}{\dot{E}x_5}$
ir Cooler	$\dot{C}_6 + \dot{C}_{19} = \dot{C}_5 + \dot{C}_{16} + \dot{Z}_{ac}$	$\frac{\dot{C}_6}{\dot{E}x_6} = \frac{\dot{C}_5}{\dot{E}x_5}, \dot{C}_{18} = 0$
Separation	$\dot{C}_{10} + \dot{C}_7 = \dot{C}_6$	$\frac{\dot{C}_{10}}{\dot{E}x_{10}} = \frac{\dot{C}_7}{\dot{E}x_7}$
Main Compressor	$\dot{C}_8 = \dot{C}_{w,comp} + \dot{C}_7 + \dot{Z}_{comp}$	$\frac{\dot{C}_{w,turb}}{\dot{W}_{turb}} = \frac{\dot{C}_{w,comp}}{\dot{W}_{comp}}$
Valve	$\dot{C}_{11} = \dot{C}_{10} + \dot{Z}_{valve}$	–
Evaporator	$\dot{C}_{12} + \dot{C}_{15} = \dot{C}_{11} + \dot{C}_{14} + \dot{Z}_{evap}$	$\frac{\dot{C}_{11}}{\dot{E}x_{11}} = \frac{\dot{C}_{12}}{\dot{E}x_{12}}, \dot{C}_{14} = 0$
Electric Compressor	$\dot{C}_{13} = \dot{C}_{w,comp,el} + \dot{C}_{10} + \dot{Z}_{comp,el}$	$\frac{\dot{C}_{w,turb}}{\dot{W}_{turb}} = \frac{\dot{C}_{w,comp,el}}{\dot{W}_{comp,el}}$
Gas Heater	$\dot{C}_1 = \dot{C}_q + \dot{C}_9 + \dot{Z}_{gh}$	$c_q = 8.75(\$/\mathrm{GJ})$[39]

A-3.2 EIRS thermoeconomic model

For the EIRS, 13 equations with 26 unknowns are produced by applying cost balance method, including exergy cost rates for heat and work streams. Similarly, the auxiliary equations are written by using the SPECO method. The cost balance and auxiliary equations of the EIRS are presented in Table A5.

Table A5
Cost balance and auxiliary equations for the EIRS.

Component	Cost balance	Auxiliary equations
Turbine	$\dot{C}_2 + \dot{C}_{w,turb} = \dot{C}_1 + \dot{Z}_{turb}$	$\frac{\dot{C}_2}{\dot{E}x_2} = \frac{\dot{C}_1}{\dot{E}x_1}$
Recuperator	$\dot{C}_3 + \dot{C}_9 = \dot{C}_2 + \dot{C}_8 + \dot{Z}_{rec}$	$\frac{\dot{C}_3}{\dot{E}x_3} = \frac{\dot{C}_2}{\dot{E}x_2}$
Mixer	$\dot{C}_4 = \dot{C}_{20} + \dot{C}_3$	–
Space Heater	$\dot{C}_5 + \dot{C}_{22} = \dot{C}_4 + \dot{C}_{21} + \dot{Z}_{spc}$	$\frac{\dot{C}_{22}}{\dot{E}x_{22}} = \frac{\dot{C}_{21}}{\dot{E}x_{21}}, \frac{\dot{C}_4}{\dot{E}x_4} = \frac{\dot{C}_5}{\dot{E}x_5}$
Air Cooler	$\dot{C}_6 + \dot{C}_{24} = \dot{C}_5 + \dot{C}_{23} + \dot{Z}_{ac}$	$\frac{\dot{C}_{24}}{\dot{E}x_{23}} = \frac{\dot{C}_5}{\dot{E}x_5}, \dot{C}_{23} = 0$
Separation	$\dot{C}_{10} + \dot{C}_7 = \dot{C}_6$	$\frac{\dot{C}_{10}}{\dot{E}x_{10}} = \frac{\dot{C}_7}{\dot{E}x_7}$
Main Compressor	$\dot{C}_8 = \dot{C}_{w,comp} + \dot{C}_7 + \dot{Z}_{comp}$	$\frac{\dot{C}_{w,turb}}{\dot{W}_{turb}} = \frac{\dot{C}_{w,comp}}{\dot{W}_{comp}}$
Ejector	$\dot{C}_{16} = \dot{C}_{11} + \dot{C}_{10} + \dot{Z}_{ejector}$	–
Phase Separation	$\dot{C}_{17} + \dot{C}_{18} = \dot{C}_{16}$	$\frac{\dot{C}_{17}}{\dot{E}x_{17}} = \frac{\dot{C}_{18}}{\dot{E}x_{18}}$
Valve	$\dot{C}_{18} = \dot{C}_{19} + \dot{Z}_{valve}$	–
Evaporator	$\dot{C}_{11} + \dot{C}_{26} = \dot{C}_{19} + \dot{C}_{25} + \dot{Z}_{evap}$	$\frac{\dot{C}_{11}}{\dot{E}x_{11}} = \frac{\dot{C}_{19}}{\dot{E}x_{19}}, \dot{C}_{15} = 0$
Electric Compressor	$\dot{C}_{20} = \dot{C}_{w,comp,el} + \dot{C}_{17} + \dot{Z}_{comp,el}$	$\frac{\dot{C}_{w,turb}}{\dot{W}_{turb}} = \frac{\dot{C}_{w,comp,el}}{\dot{W}_{comp,el}}$
Gas Heater	$\dot{C}_1 = \dot{C}_q + \dot{C}_9 + \dot{Z}_{gh}$	$c_q = 8.75(\$/\mathrm{GJ})$[39]

A-3.4 Performance assessments for base cases

In the base case scenario, the cooling output of 100 kW is targeted, the turbine inlet temperature of 500 °C, the maximum cycle pressure of 20 MPa, the minimum cycle pressure of 8.5 MPa and evaporation temperature of 5 °C are set. All assumptions for the base case scenario are presented in Table A6.

Table A6
Parameters used in the present study [24,33,40,41].

Parameter	Value
Minimum Temperature Difference Gas Heater ΔT_{min} (°C)	10
Minimum Temperature Difference Recuperator, Air Cooler Space Heater ΔT_{min} (°C)	5
Maximum Cycle Pressure P_{max} (MPa)	20
Minimum Cycle Pressure P_{min} (MPa)	8.5

(*continued on next page*)

Table A6 (*continued*)

Parameter	Value
Maximum Cycle Temperature T_{max} (°C)	500
Minimum Power Cycle Temperature T_{min} (°C)	32.3
Evaporation Temperature T_{evap} (°C)	5
Isentropic Turbine Efficiency η_{turb} (-)	0.8
Isentropic Main Compressor Efficiency η_{comp} (-)	0.7
Dead State Pressure (kPa)	101.325
Dead State Pressure (°C)	25
Refrigeration Output (kW)	100
Plant Life Time (years)	20
Annual Operation Hours (h)	8000
Interest Rate (%)	12
Maintenance Factor γ_k	0.06

The system performance under the base case scenario is given in this appendix section. The systems performance data is given in Table A7.

Table A7
Performance data of the VCRS and EIRS.

Parameter	VCRS	EIRS
W_{net} (kW)	46.5	54.43
Q_{gh} (kW)	247.32	249.83
Q_{spc} (kW)	249.27	241.95
Q_{evap} (kW)	100	100
η_{trigen} (%)	1.6	1.58
ε_{trigen} (%)	49.92	54.41
LCOE($/kWh)	0.0375	0.0366

A-3.4.1 VCRS performance. Stream data in the VCRS are given in appendix Table A8. The power consumption of the electric compressor is high due to the high pressure ratio, this leads to the low net work output of the VCRS. But still owing to the high pressure ratio, the outlet stream of the electric compressor reaches high temperature which contributes to high mixing temperature at state 4. As a result, the VCRS achieves high heating capacity and trigeneration efficiency. The exergy efficiency of the VCRS is 49.92 % because of the irreversibility associated with the expansion valve and compressors. The exergy cost rate, specific exergy costs of fuel and products, cost of exergy destruction, cost rates of components and relative cost difference of the VCRS are presented in Table A9. The expansion valve and compressors increase irreversibility, so the total cost rate of exergy destruction for the VCRS is high with a value of 3595.25$/h, the exergy cost rate of the products is 14.87$/h and specific exergy cost of products is 66.71$/GJ. Due to the relatively small system size, the costs related to components are dominated by the cost of exergy destruction. The recuperator has the highest sum $\dot{C}_D + \dot{Z}$ which is dominated by the cost of exergy destruction as shown in Fig. A1. In order to improve the thermoeconomic performance, it is suggested to use high effectiveness recuperator.

Table A8
Stream Data for the VCRS under base case.

State	$\dot{m}$ *(kg/s)*	*P (MPa)*	*T (°C)*	*h (kJ/kg)*	*s (kJ/kg.K)*	*ex (kJ/kg)*	$\dot{E}x$ *(kW)*	*c ($/GJ)*	$\dot{C}$ *($/h)*
1	1.07	20	500.00	973.29	2.66	489.29	521.39	41.06	77.08
2	1.07	8.5	411.23	879.67	2.70	385.32	410.59	41.06	60.70
3	1.07	8.5	60.32	451.41	1.80	224.30	239.01	41.06	35.33
4	1.80	8.5	63.5	457.89	1.82	225.01	405.01	47.88	69.81
5	1.80	8.5	36	319.40	1.38	216.68	390.03	47.88	67.23
6	1.80	8.5	32.3	290.52	1.29	215.80	388.44	47.88	66.95
7	1.07	8.5	32.3	290.52	1.29	215.80	229.96	47.88	39.64
8	1.07	20	55.32	312.94	1.31	232.09	247.32	52.39	46.64
9	1.07	20	311.06	741.19	2.32	359.83	383.44	52.28	72.16
10	0.73	8.5	32.3	290.52	1.29	215.80	158.48	47.88	27.32
11	0.73	3.969	5	290.52	1.32	205.93	151.24	50.18	27.32
12	0.73	3.969	5	427.48	1.82	196.08	144.00	50.18	26.01
13	0.73	8.5	68.47	467.28	1.85	226.14	166.08	57.66	34.48
14	2.67	0.5	15	63.46	0.22	1.12	2.98	0.00	0.00
15	2.67	0.5	6	25.72	0.09	3.05	8.13	59.15	1.73
16	2.39	0.5	25	105.29	0.37	0.40	0.95	85.17	0.29
17	2.39	0.5	50	209.76	0.70	4.55	10.86	85.17	3.33
18	22.45	0.12	25	424.39	3.83	14.47	324.94	0.00	0.00
19	22.45	0.12	27.3	426.71	3.84	14.48	325.14	0.33	0.38

Table A9
Results of thermoeconomic analysis of the VCRS.

Component	$\dot{C}_f$ ($/h)	$\dot{C}_p$ ($/h)	c_f ($/GJ)	c_p ($/GJ)	$\dot{C}_D$ ($/h)	$\dot{Z}$ ($/h)	$\dot{C}_D+\dot{Z}$ ($/h)	r (-)
Turbine	16.38	20.78	41.06	57.86	452.8 9	4.40	457.29	0.41
Recuperator	25.37	25.52	41.06	52.08	1456.30	0.16	1456.46	0.27
Space Heater	2.58	3.04	47.88	85.17	243.30	0.45	243.75	0.78
Air Cooler	0.27	0.38	47.88	532.94	66.57	0.11	66.68	10.13
Main Compressor	4.98	7.01	57.86	112.10	378.07	2.03	380.10	0.94
Expansion Valve	27.32	27.32	47.88	50.18	346.95	0.002	346.95	0.05
Evaporator	1.31	1.73	50.18	93.35	104.41	0.42	104.83	0.86
Electric Compressor	6.09	8.46	57.86	106.51	413.68	2.38	416.05	0.84
Gas Heater	4.82	4.91	8.75	9.89	133.12	0.09	133.20	0.13
Overall Cycle	4.82	14.87	8.75	66.71	3595.28	10.04	3605.32	6.62

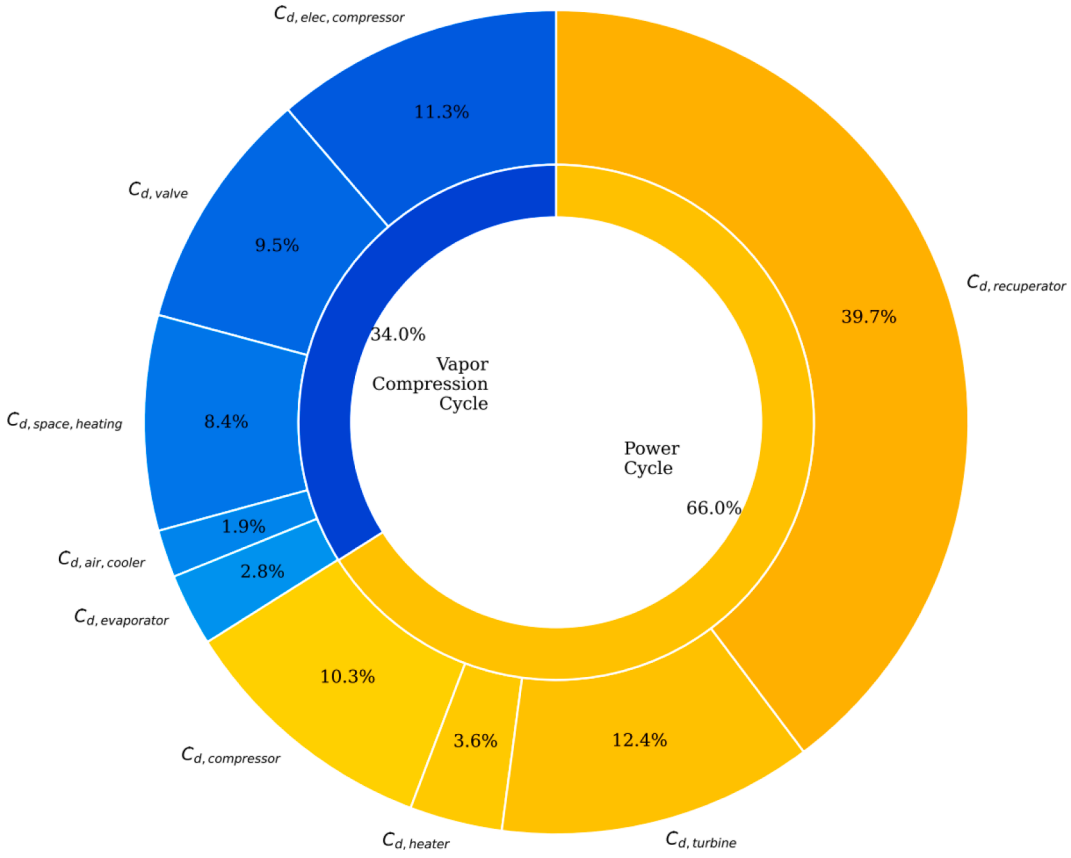

Fig. A1. Costs of exergy destruction rate for the VCRS.

A-3.4.2 EIRS performance. Stream data of EIRS is given in Table A10. Similar to the VCRS, the EIRS exergy cost rates, specific exergy costs of fuel and products, cost of exergy destruction, cost rates of components and relative cost difference are shown in Table A11. The values of 86 %, 80 % and 78 % are adopted for the nozzle and diffuser isentropic, and the mixing efficiencies respectively in the ejector [29]. Using an ejector instead of a expansion valve in the main throttling process significantly reduces irreversibility associated with the expansion process [42]. Therefore, the EIRS achieves

Table A10
Stream data for the EIRS under base case.

State	$\dot{m}$ (kg/s)	*P (MPa)*	*T* (°C)	*h* (kJ/kg)	*s* (kJ/kg.K)	*ex* (kJ/kg)	$\dot{E}x$ (kW)	*c* ($/GJ)	$\dot{C}$($/h)
1	1.076	20	500.00	973.29	2.66	489.29	526.67	35.60	67.51
2	1.076	8.5	411.23	879.67	2.70	385.32	414.75	35.60	53.16
3	1.076	8.5	60.32	451.41	1.80	224.30	241.43	35.60	30.95
4	1.800	8.5	61.48	453.82	1.81	224.55	404.20	40.21	58.52
5	1.800	8.5	36.00	319.40	1.38	216.68	390.03	40.21	56.46
6	1.800	8.5	32.30	290.52	1.29	215.80	388.44	40.21	56.23
7	1.076	8.5	32.30	290.52	1.29	215.80	232.29	40.21	33.63
8	1.076	20	55.32	312.94	1.31	232.09	249.82	44.67	40.17
9	1.076	20	311.06	741.19	2.32	359.83	387.32	44.86	62.54

(*continued on next page*)

Table A10 (*continued*)

State	$\dot{m}$ (kg/s)	P (MPa)	T (°C)	h (kJ/kg)	s (kJ/kg.K)	ex (kJ/kg)	$\dot{E}x$ (kW)	c ($/GJ)	$\dot{C}$($/h)
10	0.724	8.5	32.30	290.52	1.29	215.80	156.15	40.21	22.61
11	0.473	3.96	5.00	427.48	1.82	196.08	92.67	41.95	13.99
12	0.724	6.47	25.31	287.91	1.29	212.76	153.96	–	–
13	0.724	3.71	2.44	281.76	1.30	205.54	148.73	–	–
14	0.473	3.71	2.44	425.52	1.82	193.77	91.58	–	–
15	1.196	3.71	2.44	340.49	1.51	200.73	240.12	–	–
16	1.196	4.06	5.96	343.05	1.51	202.75	242.53	41.92	36.60
17	0.724	4.06	5.96	426.71	1.81	197.04	142.58	41.92	21.52
18	0.473	4.06	5.96	214.97	1.05	211.49	99.95	41.92	15.08
19	0.473	3.96	5.00	214.97	1.05	211.37	99.89	41.95	15.09
20	0.724	8.5	63.25	457.39	1.82	224.95	162.77	47.05	27.57
21	2.316	0.5	25.00	105.29	0.37	0.40	0.93	73.00	0.24
22	2.316	0.5	50.00	209.76	0.70	4.55	10.54	73.00	2.77
23	22.453	0.12	25.00	424.39	3.83	14.47	324.94	0.00	0.00
24	22.453	0.12	27.30	426.71	3.84	14.48	325.14	0.29	0.34
25	2.661	0.5	15.00	63.46	0.22	1.12	2.97	0.00	0.00
26	2.661	0.05	6.00	25.72	0.09	3.05	8.12	51.83	1.51

Table A11
Results of thermoeconomic analysis of the EIRS.

Component	$\dot{C}_f$ ($/h)	$\dot{C}_p$ ($/h)	c_f ($/GJ)	c_p ($/GJ)	$\dot{C}_D$ ($/h)	$\dot{Z}$ ($/h)	$\dot{C}_D+\dot{Z}$ ($/h)	r (-)
Turbine	14.35	18.78	35.60	51.76	396.66	4.43	401.09	0.45
Recuperator	22.22	22.37	35.60	45.20	1275.50	0.16	1275.66	0.27
Space Heater	2.05	2.53	40.21	73.00	183.16	0.48	183.64	0.82
Air Cooler	0.23	0.34	40.21	471.86	55.91	0.11	56.02	10.73
Main Compressor	4.50	6.54	51.76	103.63	341.63	2.04	343.68	1.00
Ejector	36.60	36.60	40.86	41.92	257.17	0.00004	257.17	0.03
Expansion Valve	15.08	15.09	41.92	41.95	2.42	0.0013	2.42	0.0007
Evaporator	1.09	1.51	41.95	81.80	87.15	0.42	87.58	0.95
Electric Compressor	4.14	6.05	51.76	83.25	104.04	1.91	105.96	0.61
Gas Heater	4.87	4.96	8.75	9.89	134.47	0.09	134.55	0.13
Overall Cycle	4.87	14.52	8.75	58.14	2838.14	9.65	2847.79	5.64

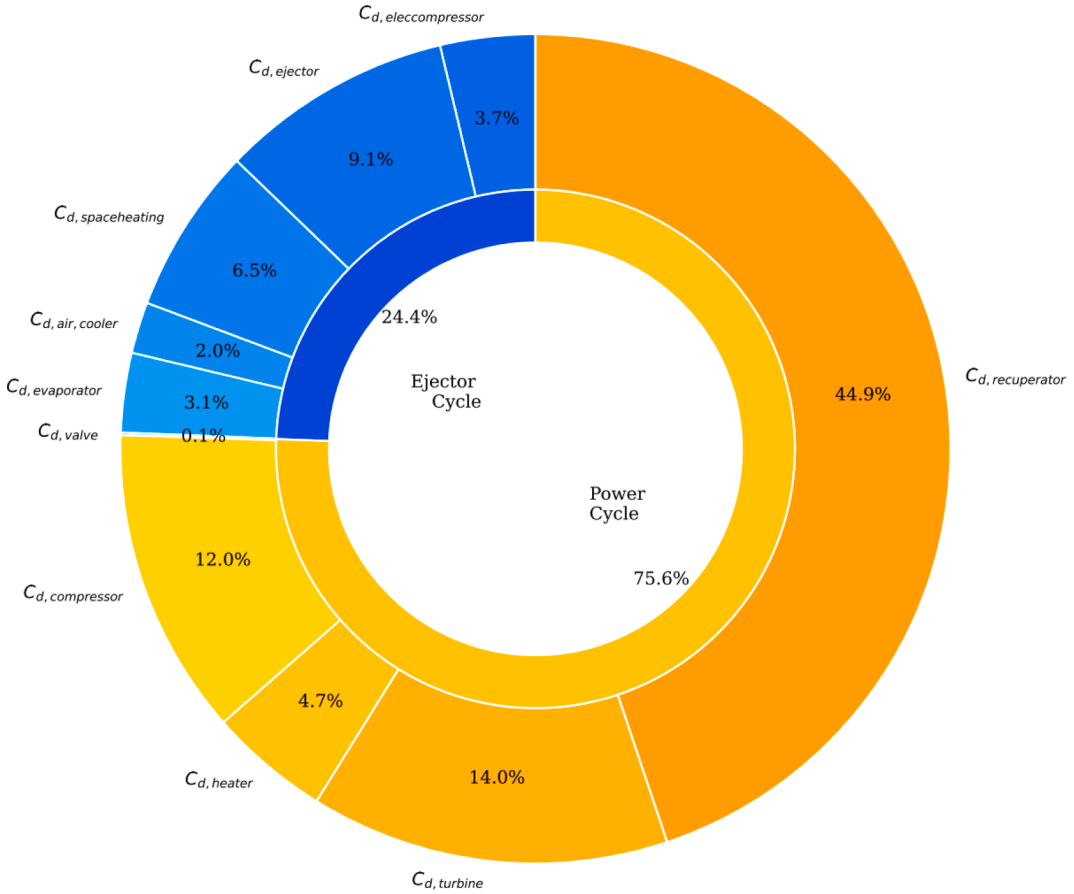

Fig. A2. Costs of exergy destruction rate for the EIRS.

relatively higher exergy efficiency compared with the VCRS, which is 54.41 %. The cost of exergy destruction rate of the EIRS is also low with a value of 2838.4$/h. The recuperator is the biggest contributor to the cost of exergy destruction rate, which accounts for 44.9 % of the total destruction rate. The electric compressor in the EIRS runs at lower pressure ratio, so the cost of exergy destruction of the electric compressor only accounts for 3.7 % of the total destruction rate, as shown in Fig. A2. Correspondingly, the exergy cost rate of products is low with a value of 14.52$/h and its specific exergy cost of products is 58.14$/GJ. The relative cost differences and sums $\dot{C}_D + \dot{Z}$ of the electric compressor and expansion valve are 0.61 and 105.96, and 0.0007 and 2.42 respectively, which are lower than those of the VCRS. For both systems, the air cooler has the highest relative cost difference, they are 10.13 for the VCRS and 10.73 for the EIRS. The outlet stream from the air cooler leads to the high exergy loss, so in order to increase thermoeconomic performance, special attention is needed for the air cooler design.

A-5 Optimization

In order to visualize decision variables and criterion space for objective functions, level diagram visualization method [43] is adopted. The level diagrams represent the objective functions and design space in Euclidean norm according to the utopia point, which help the decision makers to find the best solution. The normalized criterion and decision parameters are represented in level diagrams, as shown in Fig. A3 and A4 for VCRS and Fig. A5 and A6 for EIRS.

As can be seen from the level diagrams given in Fig. A3 and A4, the high maximum temperatures and pressures lead to the high cycle efficiency and cost rates and vice versa. Almost all optimum solutions for the VCRS are based on the evaporation temperature 5 °C where the vapour compression system performs well. Due to the big heat transfer area associated with the air cooler, all of the minimum temperature differences for the VCRS are near to the bound value of 35 °C.

Similar to the VCRS case, in the EIRS optimum solutions, the high maximum temperature and pressure result in high system efficiency and cost rates, and vice versa. Due to the ejector operation characteristics near the critical region, the optimum solutions are near the critical point for the minimum temperature difference. Compared with the VCRS, the EIRS system has higher allowance for the minimum temperature difference in heat transfer equipment.

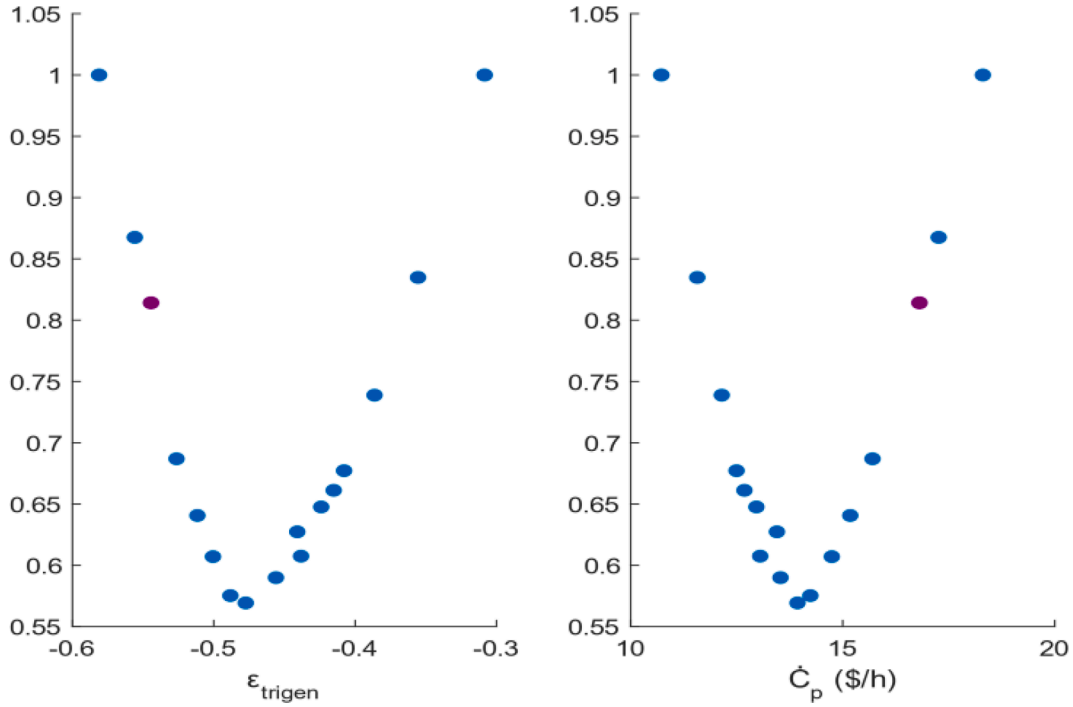

Fig. A3. Level diagrams of criterion space for the VCRS.

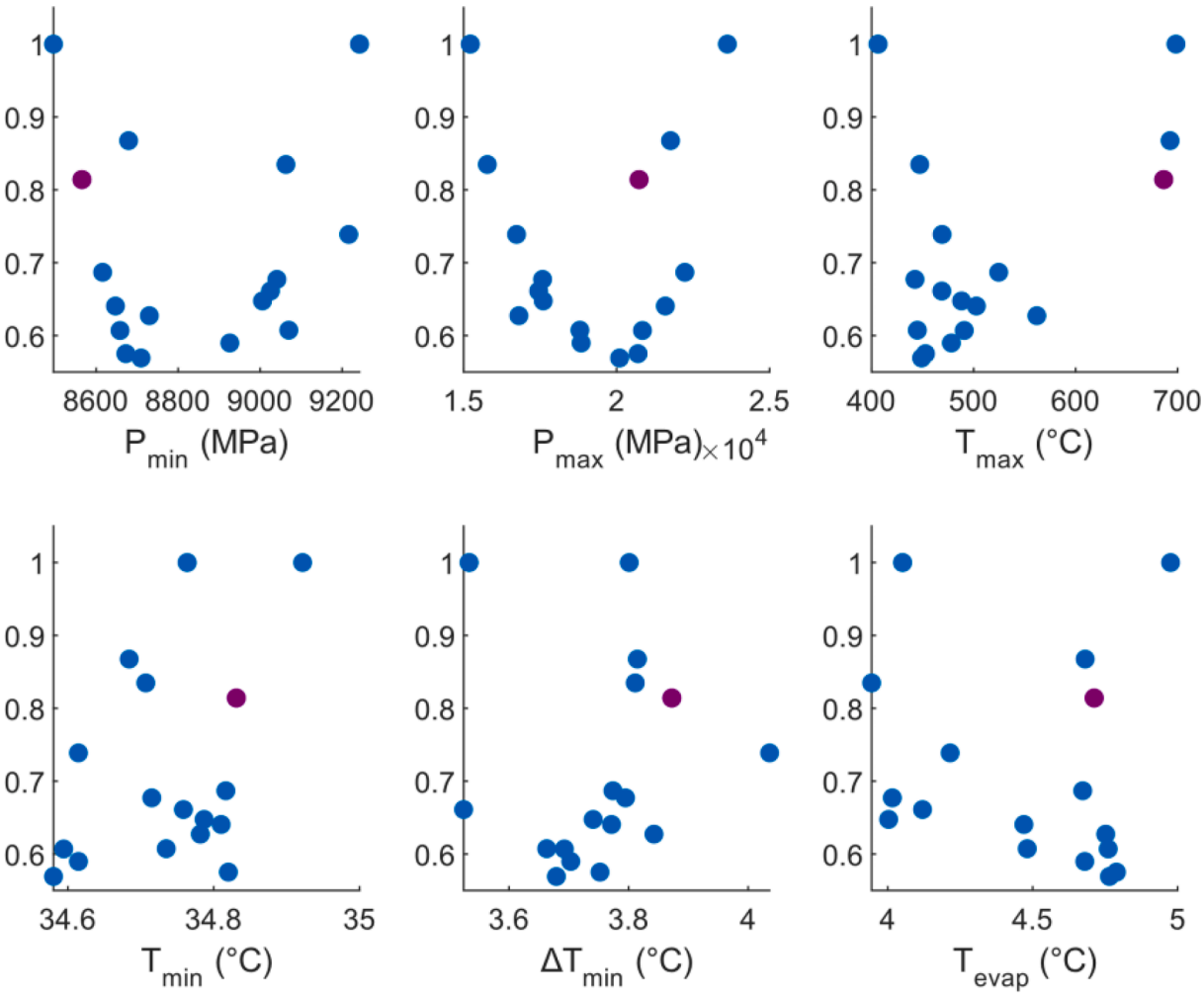

Fig. A4. Level diagrams of design space for the VCRS.

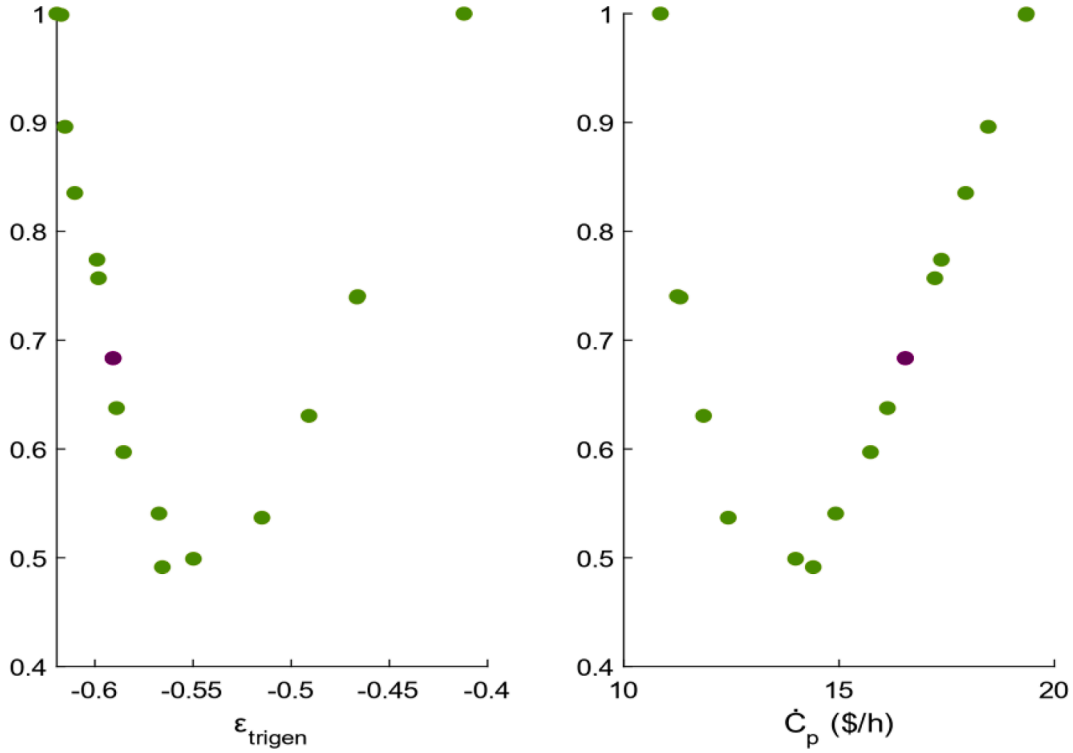

Fig. A5. Level diagrams of criterion space for the EIRS.

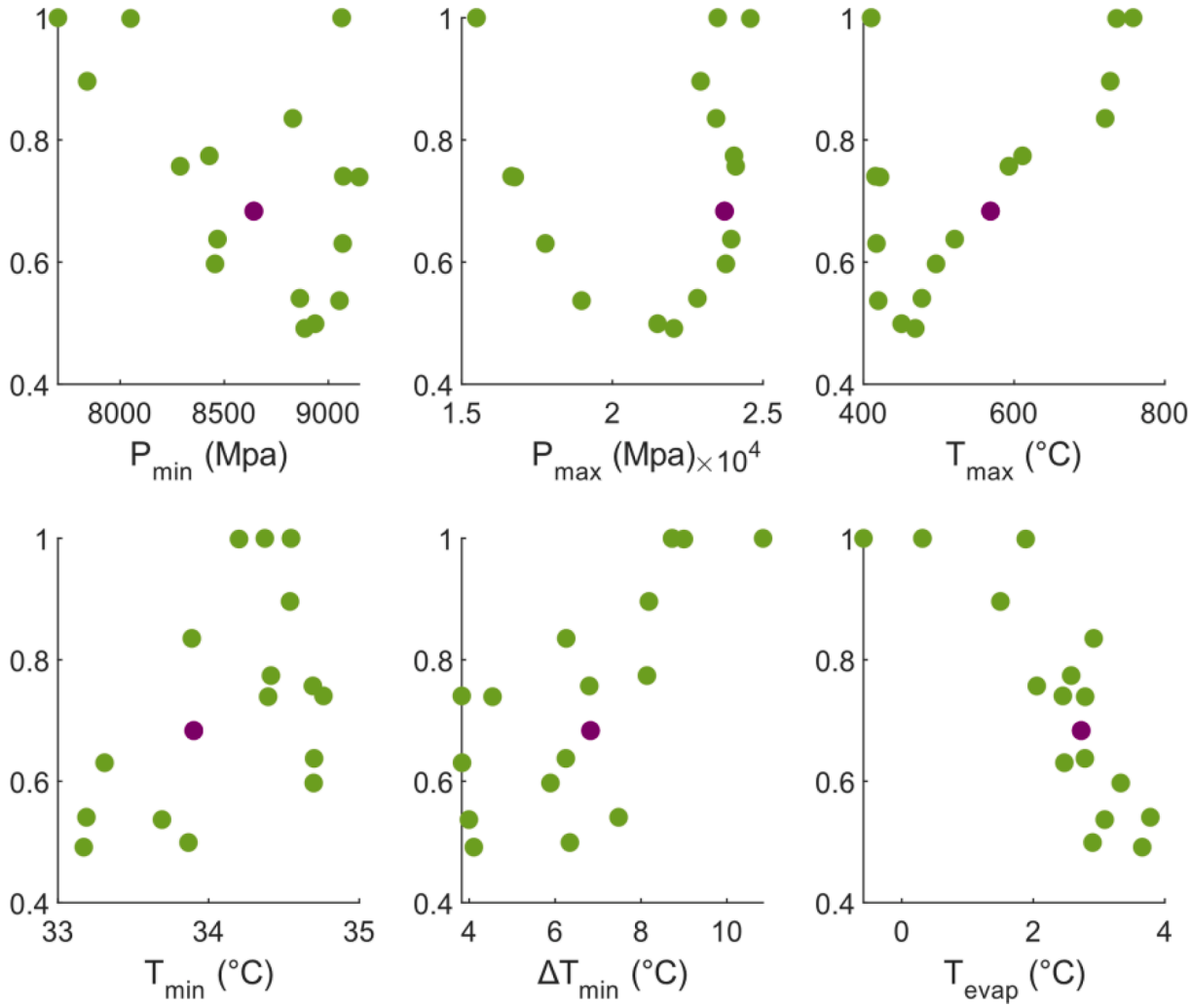

Fig. A6. Level diagrams of decision space for the EIRS.

Appendix B. Calculation procedure and model validation

B-1 Calculation procedure

The systems are modelled in MATLAB and the working fluid thermodynamic properties are calculated by using open source thermophysical property package CoolProp [44]. The system multi-layered programme is written, that feeds the results with each other's. In order to avoid the second law violation inside the heat exchanger due to the high variable nature of sCO_2 thermophysical properties around the critical region, homebrew code divides each heat exchanger into a specified number of segments and calculates the minimum temperature difference, heat transfer rate, entropy generation for each segment to get accurate sizing. Iterative process is carried out until the specified minimum temperature difference is reached. The heat transfer coefficients of the evaporator, space heater, recuperator, gas heater and air cooler are assumed as 1.5, 1.5, 2, 3 and 1.6 kW/m^2 K respectively [36–38].

In the ejector model, iterative calculations are carried out for three sections: the primary nozzle convergent section, secondary nozzle and diffuser. Calculation procedure starts with an initial entrainment ratio. In the iterative calculations, the pressure at the throat, P_{13}, is reduced until the mass flux $\rho_{13}V_{13}$ is maximized. Similarly, for the secondary nozzle outlet pressure P_{14}, Eqs. (5) and (6) are employed. To get the outlet pressure of the secondary nozzle, iterative calculations are conducted again until 0.3 Mach number at the secondary nozzle outlet is reached [24,45]. The local sound speed for the two phase flow fluid is estimated by Wood's relation [46]:

$$c^2 = \frac{1}{\rho}\frac{1}{\left(\frac{\alpha}{\rho_v c_v^2} + \frac{1-\alpha}{\rho_l c_l^2}\right)} \tag{B1}$$

where α is the void fraction and subscripts "v" and "l" represent the vapour and liquid phases respectively.

The primary nozzle divergent section outlet, state 13, can be easily calculated with the pressure at the secondary nozzle outlet. Similarly, iterative calculations are carried out for the diffuser outlet pressure P_{16} until $\rho_{16}V_{16}$ is minimized. In order to satisfy mass balance, the quality of the outlet state of the diffuser x_{16} should be equal to $(1+\mu)^{-1}$.

B-2 model validation

The model validation from the energy production aspect is conducted. For the VCRS model, the data presented by Wang et al. [19] are used. Under the same operating condition and design parameters [19], the maximum deviation between Wang's data and this study results are 5.26 % as indicated in Table B1.

The two-phase ejector model presented by Ameur et al. [24] is adopted due to the high accuracy at low evaporation temperature. Since the ejector model is validated with the *trans*-critical ejector heat pump data, the model validation of the EIRS is carried out by two groups of reference data, one is the steady-state recuperative sCO_2 cycle results [40], the other is the transcritical ejector heat pump data. The verification results are given in Table B2. It can be seen that the maximum data difference between this study and the referenced recuperative cycle is 2.78 % for the compressor specific work, while the maximum deviation between this study and the ejector heat pump is 8.75 % for the COP. Therefore, the developed models in this study can be used to investigate the VCRS and EIRS performance based on these validation results.

Table B1
Data comparison for the VCRS.

Parameter	Reference [19]	Model	Difference
W_{net} (kW)	7537.5	7537	−0.00663 %
Q_{gh} (kW)	81,945	87,561	6.41 %
Q_{spc} (kW)	34,039	35,931	5.26 %
Q_{evap} (kW)	5400	5400	–
η_{trigen} (%)	57.54	55.81	−3.09 %

Table B2
Verification results for recuperative cycle and *trans*-critical ejector heat pump.

Recuperative cycle				Trans-critical ejector heat pump			
Parameter	Reference [40]	Model	Difference	Parameter	Reference [24]	Model	Difference
Turbine specific work (kJ/kg)	125.87	124.6	1.01 %	Entrainment ratio	0.5848	0.5931	−1.42 %
Compressor specific work (kJ/kg)	20.88	20.3	2.78 %	Compression ratio	1.094	1.061	3.02 %
Specific heat input (kJ/kg)	280.39	277.47	1.04 %	COP	3.2	2.92	8.75 %
Electrical Efficiency	0.3744	0.3758	−0.37 %				

References

[1] Cao X, Dai X, Liu J. Building energy-consumption status worldwide and the state-of-the-art technologies for zero-energy buildings during the past decade. Energy Build 2016. https://doi.org/10.1016/j.enbuild.2016.06.089.

[2] Abu-Rayash A, Dincer I. Analysis of the electricity demand trends amidst the COVID-19 coronavirus pandemic. Energy Res Soc Sci 2020;68:101682. https://doi.org/10.1016/J.ERSS.2020.101682.

[3] Monzón-Chavarrías M, Guillén-Lambea S, García-Pérez S, Montealegre-Gracia AL, Sierra-Pérez J. Heating energy consumption and environmental implications due to the change in daily habits in residential buildings derived from COVID-19 crisis: the case of Barcelona, Spain. Sustainability 2021;13:918. https://doi.org/10.3390/SU13020918.

[4] Zhang D, Zhang B, Zheng Y, Zhang R, Liu P, An Z. Economic assessment and regional adaptability analysis of CCHP system coupled with biomass-gas based on year-round performance. Sustain Energy Technol Assess 2021;45:101141. https://doi.org/10.1016/J.SETA.2021.101141.

[5] Wang J, Zhao P, Niu X, Dai Y. Parametric analysis of a new combined cooling, heating and power system with transcritical CO_2 driven by solar energy. Appl Energy 2012;94:58–64. https://doi.org/10.1016/J.APENERGY.2012.01.007.

[6] Sultan U, Zhang Y, Farooq M, Imran M, Akhtar Khan A, Zhuge W, et al. Qualitative assessment and global mapping of supercritical CO_2 power cycle technology. Sustain Energy Technol Assess 2021;43:100978. https://doi.org/10.1016/J.SETA.2020.100978.

[7] Thanganadar D, Fornarelli F, Camporeale S, Asfand F, Patchigolla K. Off-design and annual performance analysis of supercritical carbon dioxide cycle with thermal storage for CSP application. Appl Energy 2021;282:116200. https://doi.org/10.1016/J.APENERGY.2020.116200.

[8] Rogalev N, Rogalev A, Kindra V, Komarov I, Zlyvko O. Structural and parametric optimization of S–CO_2 nuclear power plants. Entropy 2021;23:1079. https://doi.org/10.3390/E23081079.

[9] Chen Z, Wang Y, Zhang X. Energy and exergy analyses of S-CO_2 coal-fired power plant with reheating processes. Energy 2020;211:118651. https://doi.org/10.1016/J.ENERGY.2020.118651.

[10] Alfani D, Binotti M, Macchi E, Silva P, Astolfi M. sCO_2 power plants for waste heat recovery: design optimization and part-load operation strategies. Appl Therm Eng 2021;195:117013. https://doi.org/10.1016/J.APPLTHERMALENG.2021.117013.

[11] Vutukuru R, Pegallapati AS, Maddali R. Thermodynamic studies on a solar assisted transcritical CO_2 based tri-generation system with an ejector for dairy applications. Int J Refrig 2019;108:113–23. https://doi.org/10.1016/J.IJREFRIG.2019.08.031.

[12] Astolfi M, Alfani D, Lasala S, Macchi E. Comparison between ORC and CO_2 power systems for the exploitation of low-medium temperature heat sources. Energy 2018;161:1250–61. https://doi.org/10.1016/J.ENERGY.2018.07.099.

[13] White MT, Bianchi G, Chai L, Tassou SA, Sayma AI. Review of supercritical CO_2 technologies and systems for power generation. Appl Therm Eng 2021;185:116447.

[14] Li B, Wang S, Wang K, Song L. Comparative investigation on the supercritical carbon dioxide power cycle for waste heat recovery of gas turbine. Energy Convers Manag 2021;228:113670. https://doi.org/10.1016/J.ENCONMAN.2020.113670.

[15] Marchionni M, Bianchi G, Tassou SA. Techno-economic assessment of Joule-Brayton cycle architectures for heat to power conversion from high-grade heat sources using CO_2 in the supercritical state. Energy 2018;148:1140–52.

[16] Zhang Y, Shu G, Tian H, Shi L, Sun X. Modified CO_2-based combined cooling and power cycle with multi-mode and adjustable ability. Energy Convers Manag 2020;226:113485. https://doi.org/10.1016/J.ENCONMAN.2020.113485.

[17] Yuan J, Wu C, Xu X, Liu C. Proposal and thermoeconomic analysis of a novel combined cooling and power system using carbon dioxide as the working fluid. Energy Convers Manag 2021;227:113566. https://doi.org/10.1016/J.ENCONMAN.2020.113566.

[18] Yuan J, Wu C, Xu X, Liu C. Multi-mode analysis and comparison of four different carbon dioxide-based combined cooling and power cycles for the distributed energy system. Energy Convers Manag 2021;244:114476. https://doi.org/10.1016/J.ENCONMAN.2021.114476.

[19] Wang M, Zhang J, Liu H. Thermodynamic analysis and optimization of two low-grade energy driven transcritical CO_2 combined cooling, heating and power systems. Energy 2022;249:123765. https://doi.org/10.1016/J.ENERGY.2022.123765.

[20] Cengel YA, Boles MA, Kanoglu M. Thermodynamics: an engineering approach. 2019.

[21] Bejan A, Tsatsaronis G, Moran MJ. Thermal design and optimization. John Wiley & Sons; 1995.

[22] Wark 1927- K. Advanced thermodynamics for engineers. New York : McGraw-Hill, [1995] ©1995; n.d.

[23] Wang GB, Zhang XR. Thermoeconomic optimization and comparison of the simple single-stage transcritical carbon dioxide vapor compression cycle with different subcooling methods for district heating and cooling. Energy Convers Manag 2019;185:740–57. https://doi.org/10.1016/J.ENCONMAN.2019.02.024.

[24] Ameur K, Aidoun Z. Two-phase ejector enhanced carbon dioxide transcritical heat pump for cold climate. Energy Convers Manag 2021;243:114421.

[25] Abusoglu A, Kanoglu M. Exergoeconomic analysis and optimization of combined heat and power production: a review. Renew Sustain Energy Rev 2009;13:2295–308. https://doi.org/10.1016/J.RSER.2009.05.004.

[26] Lazzaretto A, Tsatsaronis G. SPECO: a systematic and general methodology for calculating efficiencies and costs in thermal systems. Energy 2006;31:1257–89. https://doi.org/10.1016/J.ENERGY.2005.03.011.
[27] Ebrahimi-Moghadam A, Farzaneh-Gord M, Jabari Moghadam A, Abu-Hamdeh NH, Lasemi MA, Arabkoohsar A, et al. Design and multi-criteria optimisation of a trigeneration district energy system based on gas turbine, Kalina, and ejector cycles: exergoeconomic and exergoenvironmental evaluation. Energy Convers Manag 2021:227. https://doi.org/10.1016/j.enconman.2020.113581.
[28] Suman GK, Guerrero JM, Roy OP. Stability of microgrid cluster with Diverse Energy Sources: a multi-objective solution using NSGA-II based controller. Sustain Energy Technol Assess 2022;50:101834. https://doi.org/10.1016/J.SETA.2021.101834.
[29] Abbasi HR, Pourrahmani H. Multi-objective optimization and exergoeconomic analysis of a continuous solar-driven system with PCM for power, cooling and freshwater production. Energy Convers Manag 2020:211. https://doi.org/10.1016/J.ENCONMAN.2020.112761.
[30] Chen H, Zhuge W, Zhang Y, Hongdan LIU. Effect of compressor inlet condition on supercritical carbon dioxide compressor performance. Proc ASME Turbo Expo 2019:9. https://doi.org/10.1115/GT2019-90647.
[31] Rao SS. Engineering Optimization: Theory and Practice: Fourth Edition. 2009. 10.1002/9780470549124.
[32] Arora J. Introduction to optimum design. Elsevier; 2004.
[33] Tsimpoukis D, Syngounas E, Bellos E, Koukou M, Tzivanidis C, Anagnostatos S, et al. Investigation of energy and financial performance of a novel CO_2 supercritical solar-biomass trigeneration system for operation in the climate of Athens. Energy Convers Manag 2021;245:114583. https://doi.org/10.1016/j.enconman.2021.114583.
[34] Zoghi M, Habibi H, Chitsaz A, Ayazpour M, Mojaver P. Thermo-economic assessment of a novel trigeneration system based on coupling of organic Rankine cycle and absorption-compression cooling and power system for waste heat recovery. Energy Convers Manag 2019;196:567–80. https://doi.org/10.1016/J.ENCONMAN.2019.06.030.
[35] Zare V, Rostamnejad TH. Novel geothermal driven CCHP systems integrating ejector transcritical CO_2 and Rankine cycles: Thermodynamic modeling and parametric study. Energy Convers Manag 2020. https://doi.org/10.1016/j.enconman.2019.112396.
[36] Drgoňa J, Arroyo J, Cupeiro Figueroa I, Blum D, Arendt K, Kim D, et al. All you need to know about model predictive control for buildings. Annu Rev Control 2020. https://doi.org/10.1016/j.arcontrol.2020.09.001.
[37] Ma Y, Morozyuk T, Liu M, Yan J, Liu J. Optimal integration of recompression supercritical CO_2 Brayton cycle with main compression intercooling in solar power tower system based on exergoeconomic approach. Appl Energy 2019;242:1134–54. https://doi.org/10.1016/J.APENERGY.2019.03.155.
[38] Li B, Wang S. Thermo-economic analysis and optimization of a novel carbon dioxide based combined cooling and power system. Energy Convers Manag 2019;199:112048. https://doi.org/10.1016/J.ENCONMAN.2019.112048.
[39] Noaman MB. Supercritical CO_2 cycles in combined-cycle power systems 2022.
[40] Pan M, Bian X, Zhu Y, Liang Y, Lu F, Xiao G. Thermodynamic analysis of a combined supercritical CO_2 and ejector expansion refrigeration cycle for engine waste heat recovery. Energy Convers Manag 2020;224:113373. https://doi.org/10.1016/J.ENCONMAN.2020.113373.
[41] Wang L, Pan L, Wang J, Chen D, Huang Y, Hu L. Investigation on the temperature sensitivity of the S-CO_2 Brayton cycle efficiency. Energy 2019;178:739–50. https://doi.org/10.1016/J.ENERGY.2019.04.100.
[42] Bilir Sag N, Ersoy HK, Hepbasli A, Halkaci HS. Energetic and exergetic comparison of basic and ejector expander refrigeration systems operating under the same external conditions and cooling capacities. Energy Convers Manag 2015;90:184–94. https://doi.org/10.1016/J.ENCONMAN.2014.11.023.
[43] Blasco X, Herrero JM, Sanchis J, Martínez M. A new graphical visualization of n-dimensional Pareto front for decision-making in multiobjective optimization. Inf Sci (Ny) 2008;178:3908–24. https://doi.org/10.1016/J.INS.2008.06.010.
[44] Bell IH, Wronski J, Quoilin S, Lemort V. Pure and pseudo-pure fluid thermophysical property evaluation and the open-source thermophysical property library coolprop. Ind Eng Chem Res 2014;53:2498–508. https://doi.org/10.1021/IE4033999/SUPPL_FILE/IE4033999_SI_002.ZIP.
[45] Yazdani M, Alahyari AA, Radcliff TD. Numerical modeling of two-phase supersonic ejectors for work-recovery applications. Int J Heat Mass Transf 2012;55:5744–53. https://doi.org/10.1016/J.IJHEATMASSTRANSFER.2012.05.071.
[46] Wood AB, Lindsay RB. A textbook of sound. Phys Today 1956;9:37.